Comprehensive Broken Damper Bar Fault Detection of Synchronous Generators

Hossein Ehya, *Student Member*, and Arne Nysveen, *Senior Member*

***Abstract*—Reliable operation of synchronous generators in hydroelectric power plants is crucial for avoiding unplanned stoppages that can incur substantial costs. The damper winding of salient pole synchronous generators (SPSGs) contributes to machine operation only during transient periods; however, it is a critical component that preserves the dynamic stability and protects the rotor in case of a fault. Consequently, detection of a broken damper bar (BDB) fault is vital for safe operation. Current methods for BDB detection depend on visual inspection or offline tests. However, most of the recently proposed approaches have used invasive sensors that can detect BDB faults only during transient operation. In this paper, a novel method is proposed based on a non-invasive sensor with high sensitivity to BDB faults that can identify a BDB fault either during transient operation or in the steady-state period. The effectiveness of the proposed method is validated by finite element modeling and by experimental results from a 100 kVA custom-made SPSG. The proposed method is confirmed to provide a reliable and sensitive diagnosis of BDB faults during transient or steady-state operation, even in noisy environments.**

***Index Terms*—Broken damper bar, condition monitoring, discrete wavelet transform, fault detection, salient pole synchronous generator, stray magnetic field, wavelet entropy.**

I. Introduction

SALIENT pole synchronous generators (SPSGs) are the most commonly applied generator type in hydropower plants [1], and they are ubiquitous throughout the Norwegian power generation system. The generated hydroelectric power accounts for 95% of the total electricity production in Norway [2]; consequently, the proper operation and maintenance of hydroelectric generators are essential to meet the ever-increasing operational demands. Hydroelectric generators can suffer from incipient undetected faults that may result in catastrophic damage in the long term. The failure of a SPSG and the subsequent steps required for restoration of power plant operations can create substantial expenses for the power producer.

The damper winding of the SPSG contributes to the operation of the machine both in transient and steady-state operation. It also improves the air-gap flux waveform. The transient periods of the synchronous generator includes the start-up period and the asynchronous operation due to power network transients. The damper winding protects the rotor field winding during a short circuit fault on the stator side. The damper winding also affects the generator performance in the case of load, torque, and magnetization current variations [3]–[6]. Current continuously passes through the damper winding during both transient and steady-state operations. In transient operations, the synchronous generator operates in an asynchronous mode in which the magnetic field of the rotor and stator is not synchronized. This leads to the induction of voltages inside the damper cage and a consequent circulation of current in the damper bars. Four factors cause these induced currents during steady-state operation of the machine: the air-gap magnetic field pulsation due to stator and rotor slotting effect [3], [7]; internal faults, like eccentricity and short circuits [8]; the stator load variation; and the space harmonics in the air-gap magnetic field due to the fractional slot winding layout [9].

Damper winding failure is not a prevalent type of fault in salient pole synchronous machines; however, this failure can significantly affect the performance of the machine. A broken damper bar (BDB) and a broken end ring fault in pumped storage generators, synchronous condensers, and salient pole synchronous motors are reported to cause starting failures, to reduce the efficiency of performance, and ultimately to lead to machine depreciation [10]–[12]. Damper bar breakage can occur due to a deficient connection between the dampers and the end ring, to maloperation, to numerous starts and stops, and to thermo-mechanical stress due to uneven distribution of the current inside the rotor bars because of the saliency of the rotor pole [10]–[15]. A BDB creates higher currents, thereby imposing greater mechanical and thermal tension on the remaining healthy damper bars.

The detection of a BDB fault in a synchronous machine has been mostly based on visual inspection [11]. In [16]–[18], although offline test procedures have been proposed to detect BDB faults without machine disassembly. These proposed tests are effective and show superiority over visual inspection; however, they require stoppage of the machine, as well as the use of an extra controllable power source and access to the machine winding to conduct the tests. Moreover, the rotor must be rotated manually, which is not possible for large-sized machines. In [19], an online method based on stator current harmonic analysis was introduced. However, the proposed method demonstrated a lack of sensitivity for BDB faults and

This work was supported by the Norwegian Research Centre for Hydropower Technology (HydroCen) partly funded by The Research Council of Norway (contract no. 257588).

Hossein Ehya, and Arne Nysveen are with Department of Electrical Power Engineering, Norwegian University of Science and Technology, Trondheim, 7030, Norway. (corresponding author phone: +47 47743322; e-mail: hossein.ehya@ntnu.no).

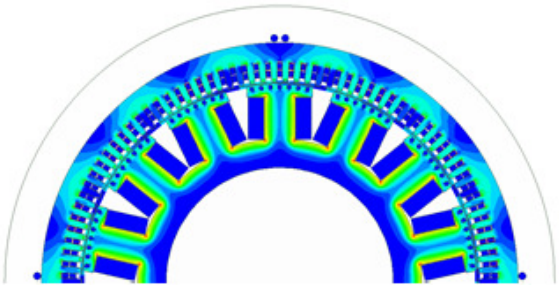

Fig. 1. The FEM of a SPSG and the location of the installed sensor for radial flux measurement on the backside of the stator yoke.

also suggested that the harmonics for BDB detection were impacted by a static eccentricity fault. Previous work [10] confirmed that a BDB altered the air-gap magnetic field during the start-up period and could increase the start-up time of the machine, but other factors, like machine loading or improper coupling of the machine, can also increase the acceleration time. The air-gap magnetic field and stator current occurring during the acceleration time has been used to detect a BDB fault in [16]–[18]. However, although the air-gap magnetic field provides detailed information about the machine status, it is an invasive approach that requires dismantling of the machine and installing a Hall-effect sensor inside the air-gap on the stator teeth. Damper bar currents [20] and end ring currents [21] have also been used to detect a BDB fault during the steady-state operation of the machine. However, these methods are not practical in reality since they require expensive sensors and data transfer equipment from the rotor side to outside the machine, in addition to a damper winding modification. In [13], a synchronous generator was operated under a 25% unbalanced load to cause a negative sequence current to circulate inside the damper winding for detection of a BDB fault; however, the proposed method is again not practical for large synchronous generators. In [22], the induced voltage in the rotor field winding during acceleration time was utilized to detect a BDB fault; however, the use of a DC power source may affect the harmonic content and mask the fault harmonics.

A comprehensive study based on the state of the art and proposed methods in the industry demonstrates a need for a non-invasive and sensitive approach for discriminating a BDB fault. The novelty of this article is encompassed below:

1) *Non-invasive* detection of a BDB fault based on the stray magnetic field
2) BDB detection during *transient* or *steady-state* operation of the SPSG
3) A novel criterion function to discriminate a BDB fault with high *sensitivity*

The finite element modeling and experimental results of a 100 kVA custom-made SPSG under a controlled fault situation are provided to validate the proposed claims.

II. Electromagnetic Analysis

This section focuses on finite element modeling (FEM) of the synchronous generator. The motivation behind the use

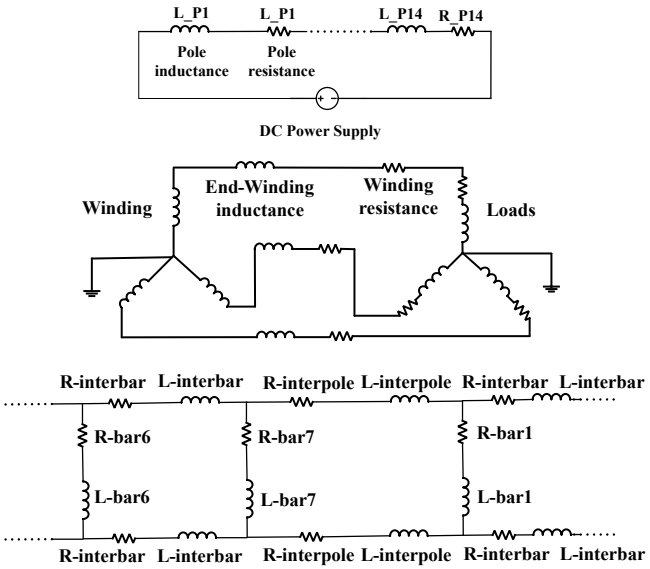

Fig. 2. The external circuit of the salient pole synchronous generator linked into a finite element, including the rotor magnetization circuit, stator windings with connected loads, and damper bar circuit connections.

TABLE I
100 kVA, 50 Hz, Synchronous Generator Topology Specification and Nameplate Data

Quantity	*Values*	*Quantity*	*Values*
No. of slots	114	No. of damper bars/pole	7
Winding connection	Wye	Number of poles	14
No. of stator turns	8	No. of rotor turns / pole	35
Nominal speed	428 rpm	Power factor	0.90
Nominal voltage	400 V	Nominal current	144.3 A
Nominal exc. current	103 A	No-load exc. current	53.2 A

of FEM is to exhibit how the current inside the bars and end rings varies in a healthy generator and in one with a single broken damper bar. Moreover, FEM is used to analyze the sensitivity of the stray magnetic field influenced by the generator configuration. FEM provides realistic results since it considers the non-linearity of the applied material in the stator and rotor core. In addition, the eddy effect is taken into account.

The FEM obtains its geometrical specification and material characteristics from a custom made 100 kVA, 400 V, 50 Hz synchronous generator with 14 salient poles. The synchronous generator under study is a 14-pole/114-slot machine with a fractional slot winding. Each rotor pole consists of 7 damper bars, which are distributed on the pole shoe. The dampers are short circuited on each side of the generator with two end rings. The connection between the rotor poles is made by the inter-pole connection rings. The two-dimensional FEM, as shown in Fig. 1, is utilized since the rotor is not skewed. The specification of the synchronous generator is presented in Table. I. The ANSYS ELECTRONICS software is used to perform FEM [23]. The ANSYS External Circuit, as shown in Fig. 2, is used to model [23]:

1) Rotor field winding
2) Stator winding and load circuit
3) Rotor damper bars and end ring circuit

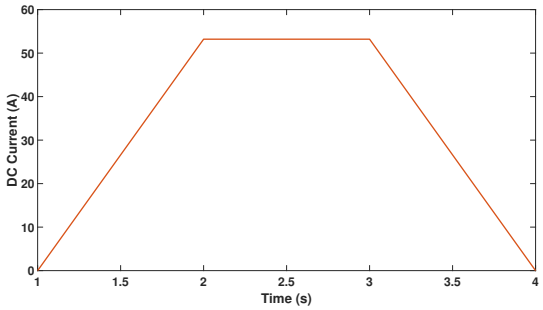

Fig. 3. The waveform of the current applied to the rotor magnetization winding of 100 kVA SPSG during no-load operation.

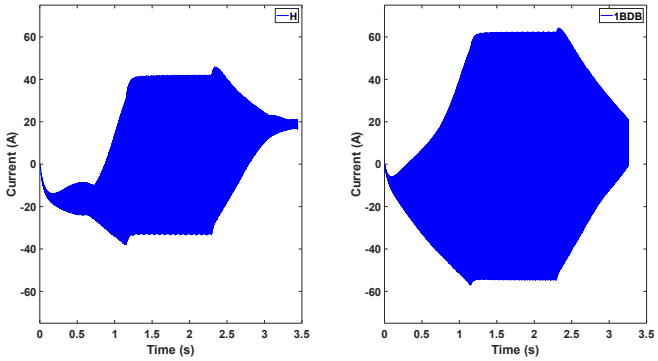

Fig. 4. The current in an inter-pole connection between two rotor poles based on an applied trapezoidal shape current at no-load at the rated speed. The left and right figures show healthy and faulty cases (one broken damper bar), respectively.

In order to show how the current inside the damper bars and the end ring changes in a healthy case and under a BDB fault, a DC current source with a controllable waveform, as shown in Fig. 3, is utilized. The synchronous generator is under constant synchronous speed when the rotor field current is increased from zero to the nominal value, which is 53.2 A. The DC source waveform consists of three sections, in which the ramp-up and the ramp-down resemble the transient behavior of the machine, while a constant DC current is fed into the winding during the steady-state (SS) operation. In order to reduce the simulation time, each period is limited to eight mechanical revolutions of the machine. An accurate simulation is achieved by using a small time step (i.e., 10 μs).

An equivalent circuit of each damper bar and end ring consists of resistance and inductance. In the case of a BDB, the resistivity of the BDB is increased to reduce the amount of the current passing through the bar. This is obtained by considering a resistance in the order of MΩ for a faulty damper bar. Fig. 4 shows the current in the end ring in a healthy case and under a BDB fault (damper No. 7 in pole one is broken). The shape of the current amplitude inside the dampers and end-rings is similar to the DC current imposed into the magnetization winding, which includes the transient and steady-state periods. The shape of the current amplitude inside the dampers differs since the location of the damper bars in the rotor shoe and their reluctance path also differ. Therefore, the shape of the current and the amplitude are different. The amplitude of the current in the bars located at the edge of the rotor pole shoe (in this generator damper bar No. 1 and No. 7) is higher than for the rest of the damper bars including damper bar No. 3, No. 4, No. 5, and No. 6. Since the reluctance of the path is higher for the bars located at the pole edge (damper bar No. 1 and No. 7, the more concentrated linkage flux is passed through the bar. The amplitude of the current decreases by reaching into the middle damper bar in the rotor pole shoe such as damper bar No. 3, No. 4, and No. 5 [22]. In the case of a BDB, the amplitude of the current in the faulty bar becomes almost zero, and the current of the adjacent bars, whether in the same pole or adjacent poles, is increased, as seen in Fig. 5 (blue and red waveforms). The amplitude of the maximum current in the adjacent faulty bar from the same pole ranges from 85 A to 100 A, while the amplitude of the maximum current bar in adjacent pole increases from 100 A to 106 A. In Fig. 5, the green and pink waveforms represent the current in three damper bars where no inter-pole connection exists and the rotor poles are separated. In the case of one BDB fault, the BDB current does not flow in the inter-pole connection and it cannot affect the damper bar's current in the neighboring poles. Therefore the damper bar current in the neighboring poles is unchanged, as shown in Fig. 5 (P2-B1 in green and pink waveforms).

TABLE II
ELECTRICAL PARAMETERS AND SPECIFICATION OF FOUR SPSGS USED FOR FEM CALCULATIONS.

Parameters	*No. 1*	*No. 2*	*No. 3*	*No. 4*
Rating power (MVA)	0.1	22	105	400
Frequency (Hz)	50	50	50	60
No. of poles	14	8	14	60
Stator outer Dia. (m)	0.78	2.64	4.54	11.27
Stator inner Dia. (m)	0.65	2.04	3.70	10.62
Stack length (m)	0.24	1.22	1.80	1.62

In a large SPSG, the poles are connected to increase the sub-transient reactance of the machine in the quadrature axis. A small sub-transient reactance in the quadrature may lead to stability problems and cause vibrations. Therefore, the connection between the poles is indispensable. The end ring current changes in the case of a BDB. The amplitude of the current in the inter-pole connection between pole one and pole two is increased from an average of 32 A in a healthy case to 56 A in the case of one BDB in pole no. 1.

A. Impact of SPSG Configuration on Stray Magnetic Field

Although the air-gap magnetic field provides accurate data for fault detection of the rotor failure, the stray magnetic field is the mirror of the air-gap magnetic field and can provide a fault-sensitive result. Four generators with different power ratings and topologies are modeled in FEM to investigate the impact of SPSG specification on the induced voltage in the installed sensor on the stator back-side. Table II shows the specification of the generators used in FEM. The FEM of the SPSG No.1 is shown in Fig. 1 while the FEM of the SPSG No.2, No. 3, and No. 4 are depicted in Fig. 6. The 100 kVA 14 poles, SPSG has an outer diameter of 0.78 m and its stack length is 0.24 m and a 400 MVA, 60 poles SPSG has an outer

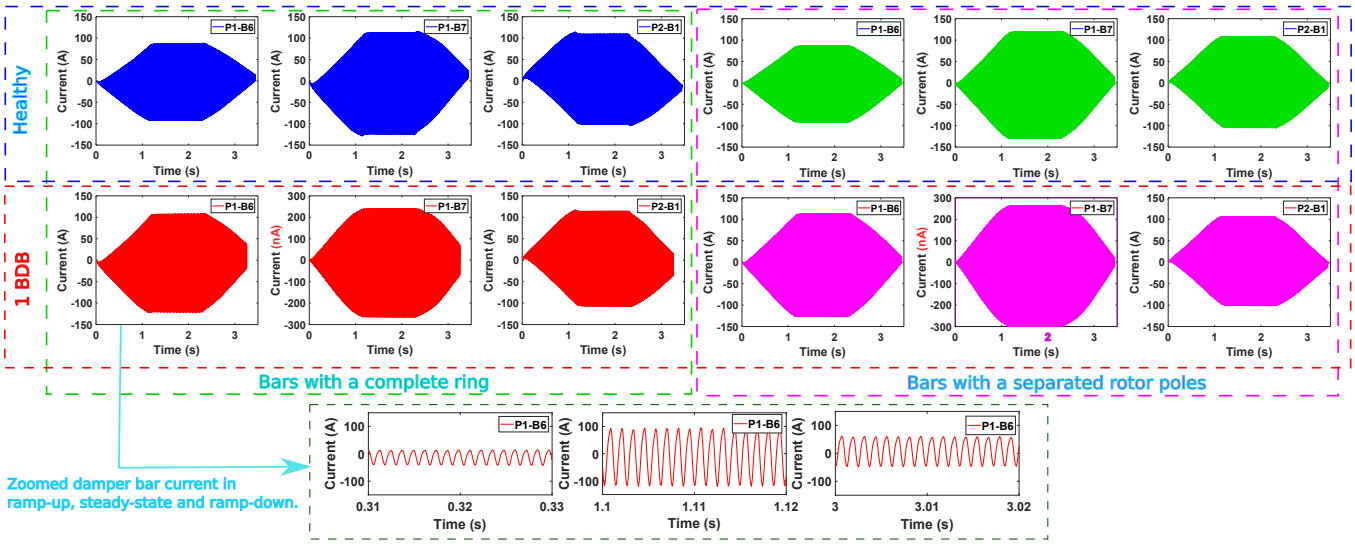

Fig. 5. Induced current in the rotor bars due to the trapezoidal shape of the field current in a healthy generator during no-load operation (blue and green waveforms) and with one broken damper bar fault (Pole #1, bar #7 (P1-B7)) (red, and pink waveforms). The first three columns are bars with a complete end ring, and the next three columns are for bars with separated rotor poles . The first three columns show the current in damper bar #6 in pole #1 (P1-B6), damper bar #7 in pole #1 (P1-B7), and damper bar #1 in pole #2 (P2-B1).

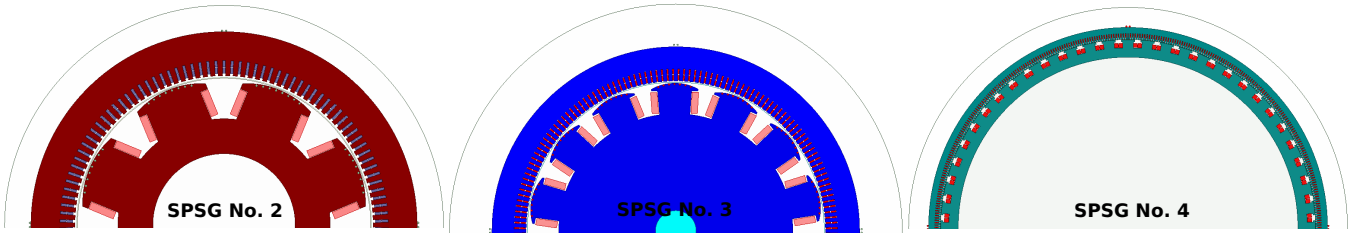

Fig. 6. The FEM of three SPSGs with different power rating and topology.

diameter of 11.27 m and its stack length is 1.62 m, are the smallest and largest modeled SPSG among the four models, respectively. Fig. 7. shows the existence of the stray magnetic field on the stator back-side of four modeled SPSGs regardless of their power rating, working frequency, number of pole pairs, the thickness and length of stator yoke, and their topologies.

III. Experimental Set-up

The test rig shown in Fig. 10 was built to execute extensive experimental tests. The fault detection system consists of a 100 kVA, 400 V synchronous generator with 14 salient poles. The nameplate data and topology specification of the SPSG are presented in Table. I. The SPSG was custom made to apply various kinds of faults, including BDB faults. The end ring and damper bars can be removed from each rotor pole. Fig. 9 shows a rotor pole, excluding the damper bars and end ring. A 90 kW, four-pole asynchronous motor drives the SPSG. The induction motor is supplied by a programmable frequency converter at the rated speed of 1482 rpm. The converter is connected to the power network. A 20 kW DC power supply (LAB-HP/E2020) is used to magnetize the rotor field windings. The connection between the SPSG and the motor is made by a gearbox.

The stray flux is captured with an in-house made sensor. The dimensions of the sensor are $(100 \times 100 \times 10)$ mm. The sensor has 3000 turns copper wire with a diameter of 0.12 mm. The resistivity and inductance of the search coil at its terminal is 912 Ω and 714 m H. The sensor is attached to the stator core and is capable of monitoring the combination of axial and radial flux. The designed sensor is cheap compared with Hall-effect sensors and it is robust to work in the industrial environment and power plants. A high-resolution 16-bit oscilloscope (Tektronix MSO 3014) with a sampling frequency of 10 kHz is used for data acquisition.

The procedure of the experimental test was as follows: the damper bar was removed at standstill, then the SPSG, which was coupled to an induction motor, accelerated until it reached synchronous speed. A trapezoid shape DC current was fed into the magnetizing circuit, as depicted in Fig. 3. As shown in Fig. 3, the DC waveform included three stages. The ramp-up and ramp-down stages were used to resemble the transient behavior of the machine, while the constant DC current was for steady-state operation of the SPSG. The period of applied DC power source for each interval was 10 seconds. The test was carried out in no-load operation of the SPSG.

IV. Signal Processing

Different time-frequency processing methods have emerged and have been applied by developing signal processing tech-

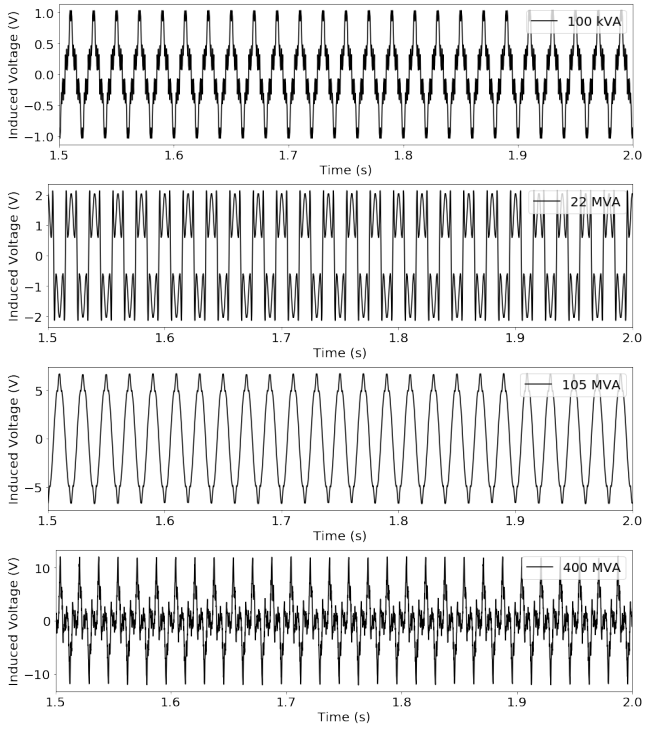

Fig. 7. The induced voltage in the sensor installed on the back-side of the stator core due to the stray magnetic field in the no-load operation of four SPSGs with different power rating and specification.

Fig. 8. The experimental test rig of a 100 kVA synchronous generator with 14 salient poles.

nology. The time-frequency analysis has become crucial, especially for a signal with non-stationary characteristics. However, extracting a feature from a non-stationary signal is a difficult task. Therefore, a tool, referred to as information entropy, is required to investigate the information contained in a signal . A quantitative assessment of the signal is obtained by applying entropy to the processed data. Discrete wavelet transforms in a combination of Shannon entropy are utilized to introduce an index for the BDB fault diagnosis. The rudimentary concept behind the wavelet entropy is consideration of the wavelet sub-bands as a probability distribution and assessment of the degree of disorder in each sub-band based on the entropy concept. The next two sections provide a brief explanation of discrete wavelet transform and Shannon entropy.

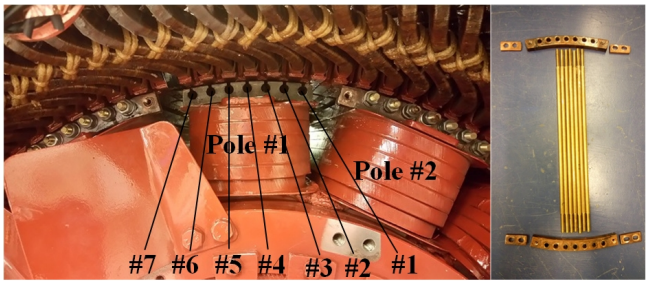

Fig. 9. The pole with the removed rotor bars and end ring (left) the salient pole synchronous generator .The removed damper bars, end rings and the inter pole connection segments (right).

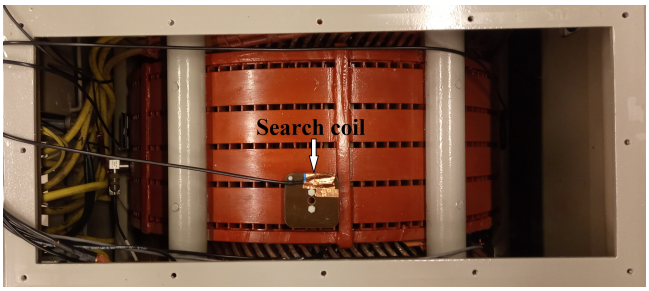

Fig. 10. The location of non-invasive search coil sensor to capture the stray magnetic field installed on the back-side of the stator yoke.

A. Discrete Wavelet Transform

The wavelet transforms of a discrete signal $S(k)$ contain the high-frequency and low-frequency components. The high frequency and low-frequency components have their own coefficients at instant k and scale i, which are denoted $d_i(k)$, and $a_i(k)$, respectively. The reconstruction of the signal frequency bands based on discrete wavelet is shown below:

$$D_i(k) : [2^{-(i+1)} f_s, 2^{-i} f_s] \tag{1}$$

$$A_i(k) : [0, 2^{(i+1)} f_s] \tag{2}$$

where i is the maximum number of scales, and f_s is the sampling frequency of the signal. The sampling frequency of the signal and the number of sub-bands determine the frequency band of the levels. The reconstructed signal $S(k)$, based on its detail and approximate decomposition, is represented below:

$$S(k) = \Sigma_{i=1}^{i+1} D_i(k) \tag{3}$$

where A_i is substituted with $D_{i+1}(k)$. The common way to implement a discrete wavelet transform is based on a bank of high-frequency and low-frequency filters. The type of mother wavelet specifies the coefficients of the high-pass and low-pass filters. Among the various types of mother wavelets utilized for feature extraction of the faulty electric machines, the Daubechies family exhibits exceptional competency for fault detection purposes. Therefore, the Daubechies mother wavelet with 8 sub-bands is used in this paper.

B. Entropy

The states and probabilities of the event determine its uncertainty. The sample space, which includes all possible sets of the state, is defined below:

$$S = s_1, s_2, s_3, ..., s_j \tag{4}$$

where the probability of each piece of information and its self-information are:

$$P(s_i) = P_i \tag{5}$$

$$\Sigma P_i = 1 \tag{6}$$

$$I(s_i) = -logP(s_i) = -logP_i \tag{7}$$

Although the self-information quantifies the whole information source, it is a random variable. Hence, it is not a suitable criterion. Consequently, to solve the random nature of the self-information, the mathematical expectation of the self-information is defined as the entropy of the information source, as below:

$$E[I(S)] = E[\Sigma logP_i] = -\Sigma P_i logP_i \tag{8}$$

The entropy gauges the uncertainty of events. In a case where whole events have the same probabilities, the uncertainty of the event and, consequently, its entropy attain maximum values. The value of the entropy is zero for any certain event.

Wavelet entropy was introduced in 1998 to process event-related potential [24]. Wavelet entropy has been used to analyze the non-stationary signal in various fields, like fault diagnosis of electric machines [25], power systems [26] and neuroscience [24]. In a case of a faulty situation, the information entropy will change, but it will not give detailed information about the frequency band that is distorted under the faulty situation. The wavelet transform, in combination with entropy, may discriminate the localized non-stationary frequencies due to the fault in each sub-band. The wavelet entropy is defined as below:

$$WE = -\Sigma_j p_j logp_j \tag{9}$$

where

$$p_j = \frac{E_{jk}}{E} \tag{10}$$

where E and E_j are the total signal energy and the energy of the each sub-band component, respectively, as defined below:

$$E_{jk} = |D_j(k)|^2 \tag{11}$$

$$E_j = \Sigma_k Ejk \tag{12}$$

V. Results

The air-gap magnetic field of a synchronous generator in the no-load condition consists of a combination of the rotor magnetic field and the damper magnetic field. In the case of a loaded generator, the stator magnetic field also contributes to shaping the air-gap magnetic field. A BDB fault in a SPSG, leads to an unbalanced distribution of the current in the damper winding and, consequently, an irregularity in the air-gap magnetic field. The stray magnetic field outside the machine mirrors the magnetic field inside the air-gap. Hence, the BDB fault in the SPSG changes the stray flux around the stator yoke. However, the modification due to the BDB fault is not only limited to the transient operation of the machine. Even during steady-state operation of the SPSG, the fault in the rotor bars alters the stray flux because current is always passing through the damper bars, as shown in Fig. 5, due to the slot harmonics or the fractional winding configuration. BDB fault detection based on stray flux monitoring using wavelet entropy is proposed since the computational complexity of the discrete wavelet transform is similar to fast Fourier transform, indicating that the proposed algorithm can be implemented online since the algorithm required computational time is limited to few seconds. The following sections describe the proposed algorithm as shown in Fig. 12

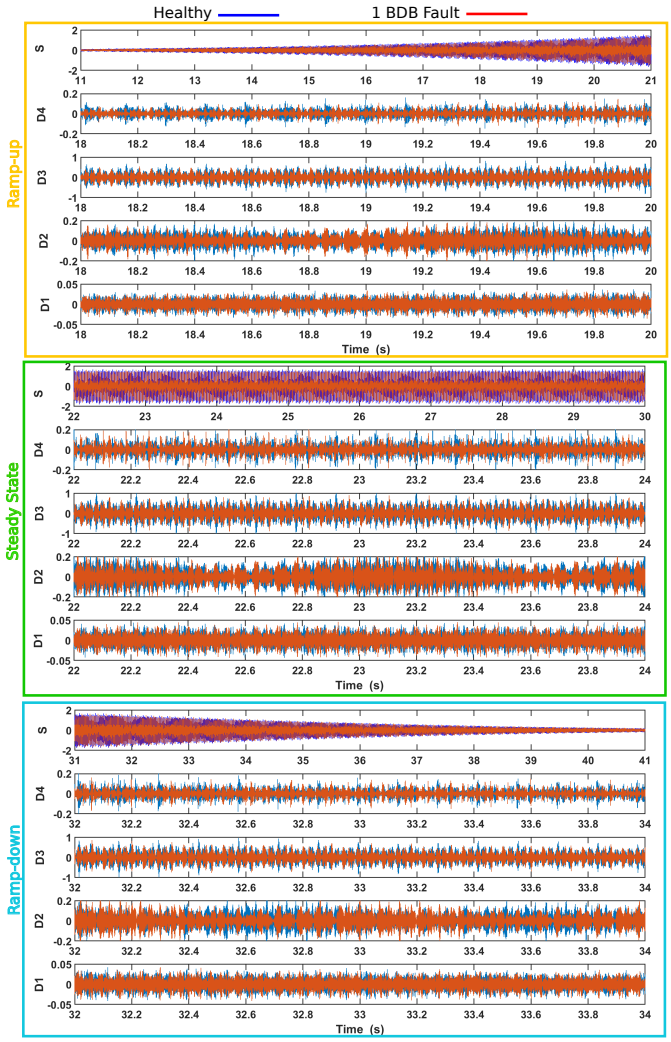

Fig. 11. The wavelet transform of the external measured magnetic field during no-load operation of the SPSG in healthy (blue) and with one BDB (red) in three cases: ramp-up (top section), steady state (middle section), and ramp-down (lower section).

TABLE III
THE VALUE OF CRITERION FUNCTION FOR FOUR WAVELET SUB-BANDS FOR DIFFERENT NUMBER OF BDB FAULTS IN THE SPSG OPERATING IN NO-LOAD CONDITION IN THREE TIME INTERVALS.

	Ramp-up interval				Steady-state interval				Ramp-down interval			
Cases	***D-4***	***D-3***	***D-2***	***D-1***	***D-4***	***D-3***	***D-2***	***D-1***	***D-4***	***D-3***	***D-2***	***D-1***
1BDB #1	15.97%	7.75%	3.37%	7.4%	18.8%	9.3%	10.1%	7.9%	37%	23.4%	17.1%	15.9%
1BDB #2	13%	7%	5.1%	1.8%	7.1%	2.4%	2.5%	1.75%	6%	1.8%	1.1%	2.9%
1BDB #4	0.6%	0.4%	2.9%	1.8%	5.1%	3.1%	3.5%	3.5%	11.36%	7.6%	6.7%	8.7%
2BDB #1 & #2	31.7%	19.4%	7.2%	1.8%	15.3%	7.3%	6.3%	0.8%	20.4%	11.4%	0.4%	5.8%
2BDB #1 & #7	25.1%	12.1%	4.2%	5.5%	13.3%	4.1%	2.0%	6.1%	20.9%	9.4%	0	4.3%
3BDB #3 & #4 & #5	7.2%	3.6%	0.2%	1.8%	3.9%	3.1%	1.45%	0	7.5%	4.5%	2.1%	1.4%
7BDB #1 to #7	31.5%	18.1%	12.1%	5.5%	29.7%	15.1%	18.8%	18.4%	44.1%	28.4%	24.1%	23.1%

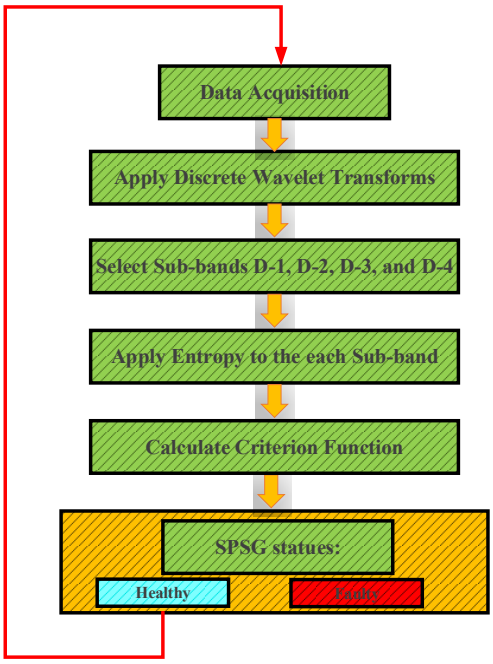

Fig. 12. Procedure of BDB fault detection in a SPSG.

A. Feature Extraction of a BDB Fault from Transient to Steady-state Operation of the SPSG

Fig. 11 demonstrates the application of the discrete wavelet transform to the acquired stray flux field. The shape of the applied magnetization current to the rotor field winding is shown in Fig. 3, but the length of the signal for ramp-up (RU), steady-state (SS), and ramp-down (RD) is a total of 40 seconds in the experimental tests. The first rows in Fig. 11 are shown with the sign 'S' to represent the acquired stray flux during the RU, SS, and RD periods, and this demonstrates how the stray flux corresponds to the magnetization current. The healthy and faulty (one broken damper bar) stray magnetic flux are colored in blue and red, respectively. Although some changes are evident in the waveform of the stray flux due to the appearance of the BDB fault, determining the degree of the fault is not possible. Therefore, the discrete wavelet transformed with the 'Daubechies' mother wavelet is used to decompose the signal into eight sub-bands. A comprehensive comparison has been done between eight sub-bands of wavelet transform in healthy and under one BDB fault. However, only four sub-bands exhibit significant differences and are detailed as sub-bands one to four, with frequency components limited between 312.5 Hz and 5 kHz for a sampling frequency of 10 kHz. The frequency band of the wavelet sub-bands D1, D2, D3, and D4 are between 5000 Hz and 2500 Hz, 2500 Hz and 1250 Hz, 1250 Hz and 625 Hz, and 625 Hz and 312.5 Hz, respectively.

Since the variation in the stray flux under a BDB fault, in comparison to a healthy case, is noticeable, the value of the signal energy and, consequently, its entropy must be different. Thus, Shannon entropy is applied to the stray flux, which is decomposed by wavelet transform. The amplitudes of the wavelet entropy for sub-bands D4 and D3 under one BDB during the RU period are increased from 405 to 482 and 6610 to 7166, respectively. The magnitude of the wavelet entropy during the RD period is also increased for the D4 and D3 sub-bands, from 382 to 607 and from 6397 to 8355, respectively, under one BDB fault. Entropy applied to the stray flux of the detailed sub-bands of D4 and D3 during steady-state operation exhibits significant changes. The magnitudes of the D4 and D3 sub-bands are increased from 959 to 1181 and from 10403 to 11473, respectively. Contrary to the assumption of a zero value for the current and, consequently, the magnetic field of the damper bars during steady-state, the obtained results questioned the proposed hypothesis.

In order to generalize the results, a new criterion function is proposed, as below:

$$CriterionFunction = \frac{|WEH_{Di} - WEF_{Di}|}{WEH_{Di}} \times 100 \quad (13)$$

where WEH_{Di}, and WEF_{Di} are wavelet entropy of corresponding wavelet sub-band in the healthy and faulty cases, respectively. The introduced criterion function is normalized by dividing by the amplitude of the healthy wavelet entropy. The first row of Table. III demonstrates the applied criterion function in the case of one BDB fault. The amplitude of the criterion function for each wavelet sub-band level differs depending on whether it occurs during transient or steady-state operation of the SPSG. The criterion function for sub-band D4 shows better sensitivity in comparison to the other sub-bands. In addition, the amplitude of the criterion function for one BDB during RD is higher than for RU and SS operation. Nevertheless, the result of applying the index to the stray flux during steady state operation also demonstrates the feasibility of BDB detection during steady-state operation.

B. Effect of the BDB Location on the Criterion Function

The rotor pole of a SPSG has a given shape in order to generate a flux waveform with minimized harmonics. Therefore, the distance of the rotor damper bars varies with respect to the stator inner diameter. The location of the damper bars imposes the magnitude of current that should pass through them, since the reluctance of their pass differs and they encounter different flux density. The amplitude of the current is higher in the damper bars located on the rotor edges than in the damper bars embedded close to the center of the rotor pole. The amplitude of the damper bar current decreases closer to the center of the rotor pole. Hence, any breakage of damper bars other than the bars at the edges has less impact on the distortion of the stray flux. Consequently, the amplitude of the criterion function is decreased for these damper bars in comparison to the damper bars at the edge. In the case of a BDB fault for damper #2, the amplitude of the criterion function becomes 13%, 7%, 5.1%, and 1.8% for wavelet sub-bands D4, D3, D2, and D1, respectively, during the RU period. The amplitude of criterion function for BDB #2 is higher during RU than during the RD period. The magnitude of the criterion function for BDB #2 is also considerable during steady-state operation, which again shows the suitability of this approach for BDB detection during the SS period. The value of the criterion function during RU and RD should not be the same due to the saturation effect since the time constant during RU is higher and it requires more magnetizing current in order to reach a partly saturated point in a B-H curve while the magnetizing current reduces and the operating point of generator changes from knee point to the linear part of a B-H curve indicating that more changes due to BDB fault are expected in the RD period.

The trickiest BDB detection is for the bar located in the middle of the rotor pole for rotors with an odd number of damper bars. The reason is that the lowest amount of current passes through this bar due to its location. Hence, its breakage has the least impact on the air-gap magnetic field distortion and, consequently, on the stray flux measured at the backside of the yoke. Table. III demonstrates how the criterion function responds to one BDB fault in the middle of the rotor pole shoe (damper #4). As already stated, the detection during the RU period is challenging because the amplitude of the wavelet entropy for all four sub-bands is not considerable. However, detection during the RD and SS period is noticeable. For instance, the amplitudes of the criterion function become 11.36% and 5.1% for sub-band D4 during the RD.

C. Multiple BDB Fault Detection

In the case of a single broken damper bar, the majority of the BDB current passes through its neighboring bars, while the cross-section of the damper bars is designed to carry the current that is designed for. Therefore, the additional current leads to a loss increment and, consequently, to a local hot spot. The result of this process in the long term is breakage of the adjacent bars. In the case of a BDB fault in two damper bars (#1 and #2), the criterion function is increased to 31.7%, 19.4%, 7.2%, and 1.8% for the D4, D3, D2, and D1 wavelet sub-bands, respectively, during RU. This shows that the amplitude of the criterion function is increased almost twofold in comparison to a single BDB fault. However, the amplitude of the criterion function is decreased for two BDB faults occurring during the SS and RD periods.

TABLE IV
THE VALUE OF THE CRITERION FUNCTION FOR FOUR WAVELET SUB-BANDS FOR ONE BDB FAULT IN A SYNCHRONOUS GENERATOR WITH SEPARATED SALIENT POLES DURING NO-LOAD OPERATION.

Periods	*Sub-band 4*	*Sub-band 3*	*Sub-band 2*	*Sub-band 1*
Ramp-up	5.5%	1.9%	1%	3.4%
Steady-state	0.1%	0.3%	0.7%	0.5%
Ramp-down	4%	5.9%	5.5%	3.3%

In the case of two BDB faults, each occurring at the corner of the same pole and exactly opposite to each other, the magnitude of the criterion function is decreased. The reason is that a symmetry exists in the non-uniform magnetic field due to the two BDB faults. As expected, the magnitude of the criterion function must be more than that for a single BDB, but less than two adjacent BDB faults. The criterion function during RU for sub-bands D4, D3, D2, and D1 is 25.1%, 12.1%, 4.2%, and 5.5%, respectively. The same trend is observed for the criterion function during the SS and RD periods.

Although increasing the number of BDBs leads to a criterion function increment, the criterion function in the case of three BDBs in the middle of the rotor pole is not considerable. The reason is that the amount of current passing through the bars in the center and its adjacent bars is less than other damper bars current and the adjacent bars of the middle bar have a symmetry in the created non-uniform magnetic field, which reduces the asymmetry of the air-gap magnetic field and the stray flux. BDB detection is possible during the RU, SS, and RD periods since a considerable increase occurs in the criterion function, especially in the D4 sub-band. In the worst case, where all damper bars of the same pole are broken, a significant increment occurs in the criterion function. The amplitude of the criterion function for all sub-bands during the RU, RD, and SS operation is increased significantly.

D. Inter-pole connection Effect on BDB Index

In large SPSGs, the damper bars are connected at both sides of the machine, either by a continuous ring or by an inter-pole connection between each pole. In a SPSG with a large number of poles, the use of a continuous ring is preferable to having an inter-pole connection since the centrifugal force acting on them may result in mechanical deformation. Removing the inter-pole connection between the poles results in a sub-transient salience (the difference between the sub transient reactance in the d and q axis), which in turn results in a huge short sub-transient circuit current in the case of a phase-to-phase short circuit fault. In addition, the induced open phase voltage in a healthy winding may increase up to twice the maximum voltage. However, some cases occur where the rotor poles are isolated and the damper bars are short circuited by the end ring in each separate pole. Removing the inter-pole connections may reduce the cost and may also avoid any damage to the

TABLE V
THE VARIATION IN THE CRITERION FUNCTION DURING STEADY-STATE OPERATION OF A SPSG UNDER DIFFERENT DEGREES OF WHITE GAUSSIAN NOISE

Noise Level	*Sub-band 4*	*Sub-band 3*	*Sub-band 2*	*Sub-band 1*
No-noise	18.8%	9.3%	10.1%	7.9%
80 dB	18.6%	9.3%	10.1%	7.9%
60 dB	18.7%	10.2%	10%	7%
40 dB	19.9%	10.3%	9.9%	6.8%
20 dB	19.6%	9.6%	6.5%	0.4%

SPSG, since the centrifugal force causes deformation in the long run.

The proposed method and the criterion function have been applied to a SPSG without inter-pole connections. Table. IV shows the result for a case of a single BDB fault (bar #1 was removed). The amplitude of the criterion function did not increase significantly, unlike the case of a rotor with a continuous ring. The amplitudes of the D4, D1, and D4 to D1 sub-bands during RU and RD were increased; however, their increments are similar to those of the BDB fault in bar #4 in a case with a continuous ring. The results obtained from steady-state operation show that detection of a BDB fault is almost impossible during this period. The reason is that the current in the damper bar circulates between the poles. In the case of isolated poles, no circulating current exists between the poles and the BDB fault cannot significantly distort the magnetic field and, correspondingly, the stray flux.

E. Noise Effect on Index

A desirable data set without noise interference is preferable for signal processing of faulty electric machines, as noise may mask the fault indices or give a false positive fault signal. Various kinds of noise may exist in a power plant, with the most prevalent kind being white Gaussian noise. Fig. 13 shows the measured noise in a Norwegian hydropower plant. Therefore, the appearance of noise in the measured data is unavoidable, and its effect on the proposed feature criterion must be studied. An analysis of the measured data in the power plant demonstrate that the existing type of noise is white Gaussian noise with a signal-to-noise ratio of 75 dB.

The proposed criterion function was also investigated under impact of white Gaussian noise with different ratio levels of 80 dB, 60 dB, 40 dB, and 20 dB. The proposed criterion function is not robust to the noise effect during the transient operation of the SPSG. The amplitude of the criterion function for sub-band D4 during RU and RD changed from 15.9% and 37% in a no-noise situation to 33.4% and 20.7% with 20 dB noise. This result shows that detection during RU and RD is impossible for a SPSG operating in environment with a noise ratio above 20 dB, even though the amplitude of the criterion function for steady-state operation is unchanged. Table. V shows the results for the criterion function under a noise effect during steady-state operation. As seen in Table. V, the amplitude of the index is almost unchanged.

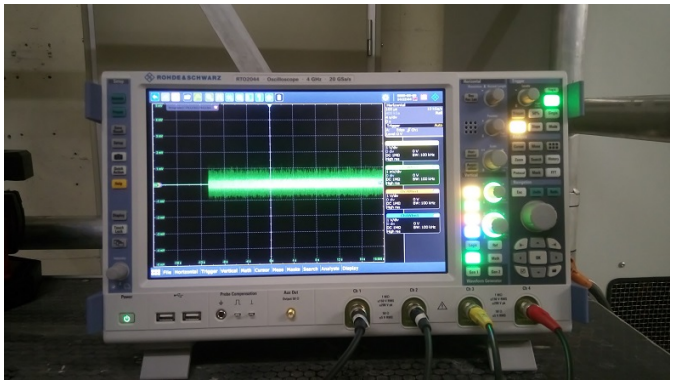

Fig. 13. Measured Noise in a Hydro-power Plant.

VI. CONCLUSION

A novel approach is proposed for the diagnosis of BDB faults in a SPSG. A trapezoidal shape current is utilized as a rotor power source that includes RU, SS, and RD regions that are symbols of transient and steady-state operation of the SPSG. The criterion function is introduced based on wavelet entropy analysis of the stray magnetic field for accurate BDB detection.The detection is not limited to the transient operation of the SPSG, and it can diagnose a fault with high sensitivity even during steady-state operation. The obtained criterion function in RU, SS, and RD are complementary features for BDB detection in the way that if the operator finds any increment in criterion function in one of the operating regions, the should check the criterion function for the other operating conditions in order to avoid a false alarm. The location of the BDB fault has a significant impact on the magnitude of the criterion function since the amplitude of the current that passes in the damper bars depends on the location of the damper bar in the rotor pole shoe. Measurement in a power plant shows that the operating environment of synchronous generators is vulnerable to noise. Therefore, the efficacy of the proposed index is examined and is deemed robust to a high rate of noise that indicates the method's reliability.

The experimental results for a small-scaled 100 kVA salient pole synchronous generator running in a Norwegian hydropower plant verified the feasibility of using the proposed method for BDB fault diagnosis. The method has no need for machine disassembly to install sensors inside the machine. The high sensitivity of the method is demonstrated, even for the detection of a middle broken bar. Detection is also possible during both transient and steady-state operation of the machine, demonstrating the superiority of the proposed method over existing methods. The proposed method is based on the no-load operation of the SPSG. BDB detection for a loaded SPSG is only possible during SS operation since the generator cannot connect to the grid before it reaches the nominal voltage. The criterion function for a loaded SPSG must be performed in the same magnetization current in the healthy and faulty cases since the variation in the stray magnetic field is influenced by the loading condition.

REFERENCES

[1] D. P. Kothari and I. J. Nagrath, *Electric Machines*. Tata McGraw-Hill Education, 2004, google-Books-ID: axGw7r3SOEMC.

[2] "08583: Elektrisitetsbalanse (MWh) 2010m01 - 2019m09." [Online]. Available: http://www.ssb.no/statbank/table/08583/

[3] G. Traxler-Samek, T. Lugand, and A. Schwery, "Additional losses in the damper winding of large hydrogenerators at open-circuit and load conditions," *IEEE Transactions on Industrial Electronics*, vol. 57, no. 1, pp. 154–160, 2009.

[4] R. Wamkeue, I. Kamwa, and M. Chacha, "Line-to-line short-circuit-based finite-element performance and parameter predictions of large hydrogenerators," *IEEE Transactions on Energy conversion*, vol. 18, no. 3, pp. 370–378, 2003.

[5] J. Machowski, J. Bialek, J. R. Bumby, and J. Bumby, *Power system dynamics and stability*. John Wiley & Sons, 1997.

[6] A. M. Knight, H. Karmaker, and K. Weeber, "Use of a permeance model to predict force harmonic components and damper winding effects in salient pole synchronous machines," in *IEMDC 2001. IEEE International Electric Machines and Drives Conference (Cat. No.01EX485)*, pp. 179–184, 2001.

[7] J. Matsuki, T. Katagi, and T. Okada, "Effect of slot ripples on damper windings of synchronous machines," in *[1992] Proceedings of the IEEE International Symposium on Industrial Electronics*, pp. 864–865. IEEE, 1992.

[8] C. Bruzzese and G. Joksimovic, "Harmonic signatures of static eccentricities in the stator voltages and in the rotor current of no-load salient-pole synchronous generators," *IEEE Transactions on Industrial Electronics*, vol. 58, no. 5, pp. 1606–1624, 2010.

[9] M. Ranlöf and U. Lundin, "The rotating field method applied to damper loss calculation in large hydrogenerators," in *The XIX International Conference on Electrical Machines-ICEM 2010*, pp. 1–6. IEEE, 2010.

[10] H. C. Karmaker, "Broken damper bar detection studies using flux probe measurements and time-stepping finite element analysis for salient-pole synchronous machines," in *4th IEEE International Symposium on Diagnostics for Electric Machines, Power Electronics and Drives, 2003. SDEMPED 2003.*, pp. 193–197, 2003.

[11] P. J. Berry and E. S. Hamdi, "An investigation into damper winding failure in a large synchronous motor," in *2015 50th International Universities Power Engineering Conference (UPEC)*, pp. 1–4, 2015.

[12] S. K. Sahoo, P. Rodriguez, and M. Sulowicz, "Comparative investigation of fault indicators for synchronous machine failures," in *2014 International Conference on Electrical Machines (ICEM)*, pp. 1503–1509, 2014.

[13] J. Bacher, "Detection of broken damper bars of a turbo generator by the field winding," *Renewable energy power quality journal*, vol. 1, pp. 199–203, 2004.

[22] H. Ehya, A. Nysveen, R. Nilssen, and U. Lundin, "Time domain signature analysis of synchronous generator under broken damper bar fault," in *IECON 2019 - 45th Annual Conference of the IEEE Industrial Electronics Society*, vol. 1, pp. 1423–1428, 2019.

[14] J. A. Antonino-Daviu, M. Riera-Guasp, J. Pons-Llinares, J. Roger-Folch, R. B. Perez, and C. Charlton-Perez, "Toward condition monitoring of damper windings in synchronous motors via emd analysis," *IEEE Transactions on Energy Conversion*, vol. 27, no. 2, pp. 432–439, 2012.

[15] H. Karmaker and Chunting Mi, "Improving the starting performance of large salient-pole synchronous machines," *IEEE Transactions on Magnetics*, vol. 40, no. 4, pp. 1920–1928, 2004.

[16] J. Yun, S. W. Park, C. Yang, S. B. Lee, J. A. Antonino-Daviu, M. Sasic, and G. C. Stone, "Airgap search coil-based detection of damper bar failures in salient pole synchronous motors," *IEEE Transactions on Industry Applications*, vol. 55, no. 4, pp. 3640–3648, 2019.

[17] J. Antonino-Daviu, V. Fuster-Roig, S. Park, Y. Park, H. Choi, J. Park, and S. B. Lee, "Electrical monitoring of damper bar condition in salient-pole synchronous motors without motor disassembly," *IEEE Transactions on Industry Applications*, vol. 56, no. 2, pp. 1423–1431, 2020.

[18] Y. Park, S. B. Lee, J. Yun, M. Sasic, and G. C. Stone, "Air gap flux-based detection and classification of damper bar and field winding faults in salient pole synchronous motors," *IEEE Transactions on Industry Applications*, vol. 56, no. 4, pp. 3506–3515, 2020.

[19] P. Neti, A. B. Dehkordi, and A. M. Gole, "A new robust method to detect rotor faults in salient-pole synchronous machines using structural asymmetries," in *2008 IEEE Industry Applications Society Annual Meeting*, pp. 1–8, 2008.

[20] F. Holmgren, "Damper winding fault detection in synchronous machines," *Master Thesis University of Uppsala*, p. 54, Nov. 2016.

[21] P. Rodriguez, "Method and a diagnostics device for determining a fault condition in a synchronous motor," *Euro Patent EP3401693*, Nov. 2018.

[23] ANSYS®, "Academic Research Electronics Desktop," Release R2.4.

[24] O. A. Rosso, S. Blanco, J. Yordanova, V. Kolev, A. Figliola, M. Schurmann, and E. Basar, "Wavelet entropy: a new tool for analysis of short duration brain electrical signals," *Journal of Neuroscience Methods*, vol. 105, DOI https://doi.org/10.1016/S0165-0270(00)00356-3, no. 1, pp. 65 – 75, 2001. [Online]. Available: http://www.sciencedirect.com/science/article/pii/S0165027000003563

[25] I. Zamudio-Ramirez, R. A. Osornio-Rios, R. d. J. Romero-Troncoso, and J. A. Antonino-Daviu, "Wavelet entropy to estimate the winding insulation healthiness in induction motors," in *IECON 2019 - 45th Annual Conference of the IEEE Industrial Electronics Society*, vol. 1, pp. 3716–3722, 2019.

[26] H. Zheng-you, C. Xiaoqing, and F. Ling, "Wavelet entropy measure definition and its application for transmission line fault detection and identification; (part ii: Fault detection in transmission line)," in *2006 International Conference on Power System Technology*, pp. 1–5, 2006.